Test of a Flux Modulation Superconducting Machine for Aircraft

Alexandre Colle, T. Lubin, Sabrina Ayat, Olivier Gosselin, Jean Lévêque

Journal of Physics: Conference Series

Test of a Flux Modulation Superconducting Machine for Aircraft

Test of a Flux Modulation Superconducting Machine for Aircraft

A Colle[2], T. Lubin[1], S. Ayat[2], O. Gosselin[2], J. Leveque[1]

1 Université de Lorraine, Research Group in Electrical Energy, 54506, Vandoeuvre, France
2 SAFRAN Tech, 78114, Magny les hameaux, France

Abstract. The increasing of drives towards More Electric Aircraft (MEA) or the development of electric propulsion aircraft calls for MW-class electrical machines with more compact and power dense designs. One way is to explore the use of superconducting (SC) materials to create a high magnetic field in order to reduce the mass of ferromagnetic components. This paper presents the design and the test of a brushless axial flux superconducting machine. The brushless topology satisfies the aeronautics industry requirements in terms of maintenance, while the axial configuration ensures an optimal use of the anisotropic HTS tapes. The machine is classed as partially superconducting, only the inductor is made with superconducting materials. A 50kW prototype is manufactured with a minimal mass objective. The prototype constitutes a first step to a scale-up MW-class machine design.

1. Introduction

Five electrical architectures are currently available for a possible electrical propulsion aircraft [1]. These technologies pro-vide reduced fuel burn, noise, and greenhouse gas emission due to the combustion of the fossil fuel. The turboelectric con-figuration is currently one of the most popular electrical architectures for the air-transportation of tomorrow. In a turboelectric airplane, the electrical generators convert the turboshaft power into electrical power, which is then distributed to several electrical motors that drive the fans. Hence, electrical storage systems are no longer required for this architecture. However, the efficiency of this structure strongly depends on the power density of the electrical machines, and on its integration with a boundary layer ingestion (BLI) design.
In parallel, the MEA is developed by the aerospace industry. It consists of replacing all currently pneumatic, hydraulic and mechanical systems by electrical devices. So, the electric power need will continue to increase through the next generation of aircraft. Different projects and their objectives are listed in the Table I [2]. In the literature, several researches have been completed concerning the SC machines in aeronautics [3]-[7]. One main observation was that this disruptive technology could reach a higher power-to-mass ratio when integrated into electrical machines.

This paper is focused on the design and test of a partially superconducting electrical machine, called flux modulation machine. For this machine, High Temperature Superconductors (HTS) are used. These superconductors are chosen be-cause of an accessible price and a lighter refrigeration system compared to a machine using low temperature superconductors. The topology of the studied machine is described in Fig. 1. The design resulted in a brushless axial flux machine. One of the key design objectives was to avoid all the maintenance and safety issues of a brush system and the additional weight of a rotating diode system. As shown in Fig. 1, superconductors are present exclusively in the inductor. A solenoid coil is composed by HTS tapes, which create a magnetic field along the axial direction. HTS

pellets, also called magnetic shields, obtain the field modulation. The principle of the modulation is explained in details in section II of this paper. A three-phases copper winding placed on each side of the pellets composes the armature winding. The flux crossing the copper winding change when shields are rotating, which induces a back-electromotive force to the armature winding terminals.

The first part of the article describes the design of the SC machine and the different technical choices made during manufacture. In a second part, the test bench of the SC ma-chine is shown. We will also see all the instrumentation used for the tests. Finally, in the last part, the first electrical tests are presented. It includes the validation of magnetic flux modulation compared to our numerical models. Then a no-load test is realized to visualize the voltage induced during the rotation of the machine.

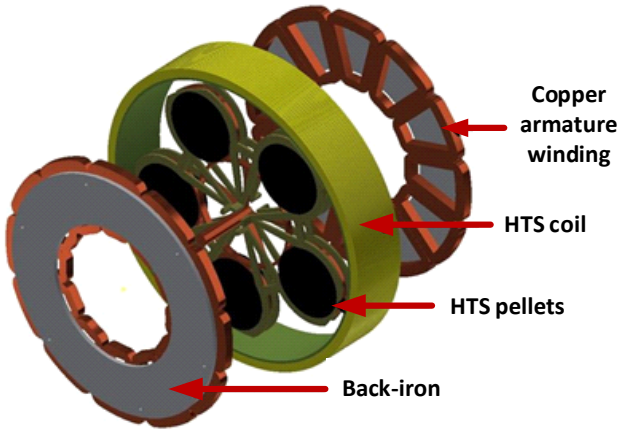

Figure 1. Exploded view of the superconducting machine's active components

Table 1. Electrical propulsion aircraft projects [2].

Project name	Electric architecture	Electrical power (MW)	PtM (kW/kg)
BOEING SUGAR	Parallel hybrid	Motor: 5,3	5
NASA N3X	Turboelectric	Generator: 30 Motor: 4	10 10
ESAero	Turboelectric	Generator: - Motor: -	8 5

2. Design of the superconducting machine

2.1. Flux modulation principle

As exposed previously, this prototype is classed into the partially SC machine because the armature winding is made with copper conductors. This choice is based on a study concerning the significant AC losses in a SC machine occurring with the current technology of HTS tapes or wires and the rotating speed of an aircraft application [8].

The flux modulation is obtained with two parts of the SC inductor, which are:

- An HTS coil built with the first generation of HTS tape (Sumitomo new type H DI-BSSCO®). In this element circulates a DC current that produces an axial magnetic field.
- Several HTS pellets are used to modulate the magnetic flux density. The diamagnetic behaviour of the bulks is used to deviate the flux lines obtained with the HTS coil, like a magnetic shield.

So, the SC inductor is the combination of the HTS coil and the HTS pellets. The magnetic flux density distributions over one pole and the distribution of the current density into the SC pellet are shown in figure 2. These numerical results are obtained with an H-formulation implemented in the COMSOL

Multiphysics software [9]. In this simulation, the HTS coil is sup-plied with the critical current obtained from the magnetic constraint seen by the conductor while a power law model is used to describe the nonlinear resistivity of the HTS pellets (a current density J=500 A/mm² with a n-factor of 25 is considered in this simulation). The flux modulation appears when every SC element are cooled below their critical temperature, then the HTS coil is slowly supplied to the critical current. During this step, the Lenz- law into the HTS pellets induces a current, it appears a low field zone just behind a shield and a high field zone between them.

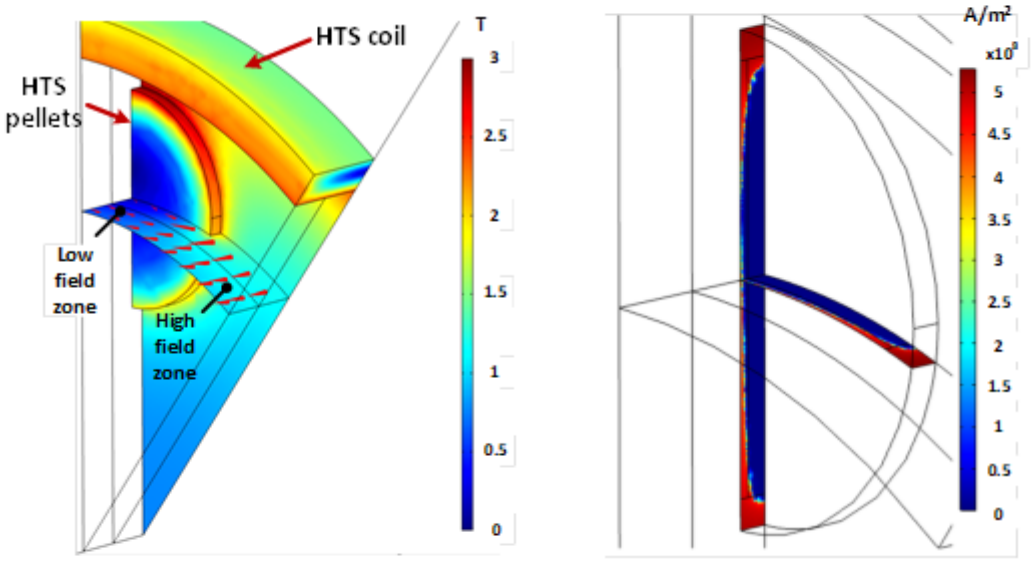

Figure 2. Magnetic field distribution behind a HTS bulk

2.2. Overview

The design parameters for the 50 kW HTS motor are summarized in Table 2. Cooling is provided by a helium circulation with an operating temperature of 30K. The dimensions of the machine were obtained with an optimization, based on a semi-analytical model of the inductor magnetic behaviour [10]. The main objective of the design was to reduce the mass of the SC machine. figure 1 shows the active components, while figure 3 and 4 represent respectively the assembled HTS motor and the rotor with the HTS pellets. The current power-to-mass ratio of the machine is slightly lower than 1 kW/kg. Even if aluminium was used for the cryostats, in order to reduce mass, significant safety margins were taken. These decisions have significantly increased the mass of the HTS machine.

2.3. Rotor structure

In order to have a brushless machine, the HTS coil is static. The rotor consists of a fiberglass/epoxy composite (G10) wheel with the HTS pellets and a titanium support. The SC pellets see the mechanical stress. So, the mechanical shaft is thermally insulated by the G10 and a special design of a Ti6A14V support, titanium alloy with a low thermal conductivity.

The material chosen for the shields is YBCO. The radius of the pellets is 40 mm for a thickness of 10 mm. The company ATZ, which manufactured the 5 pellets, only produces it using several germs for such sizes. For these one, 4 germs were used per pellet.

The SC pellets are inserted in copper rings, that we can see in Fig 4. The thermal contact is ensured by tightening these rings. A copper pipe in which the cold helium circulates is soldered to the various rings.

2.4. Stator structure

In line with the reduction of mass criterion, a double-layer concentric winding is chosen. Concentrated windings have a shorter end-winding length compared to distributed windings, this shortening reduces

weight [11]. There is no ferromagnetic tooth, so the armature windings are not protected against flux change. This is why a rectangular type-8 Litz wire was used to reduce eddy-current losses while conserving a good filling factor.

A thin hollow cylinder of laminated Si-Fe is used as a sup-port for armature windings. It has been shown that this thin back-iron increase the magnetic flux density in the air-gap and therefore the torque of the machine without being too heavy. The power-to-mass ratio is thus increased.

2.5. Cryogenic cooling system

To cool down the rotor, we used a closed loop of helium gas under pressure, 18 bar. This cooling system is composed by a CP1110 helium compressor package from Cryomech which supply an AL325 cold head (Gifford-MacMahon type). An-other compressor, CP380, is used at room temperature to in-sure the flow of helium cooled by the cold head. The cooling system is able to extract 30W of losses at 20K and 80W of losses at 30K [12].

Table 2. Design parameters of the 50 kW prototype.

Type	Value
Designed power	50 kW
Designed rotating speed	5000 rpm
Pole pairs	5
Rated armature voltage	230 V
Rated armature current	72 A
Total mass	52 kg
Operating temperature	30 K
HTS coil critical current	230 A
Outer diameter	400 mm
Total length	200 mm

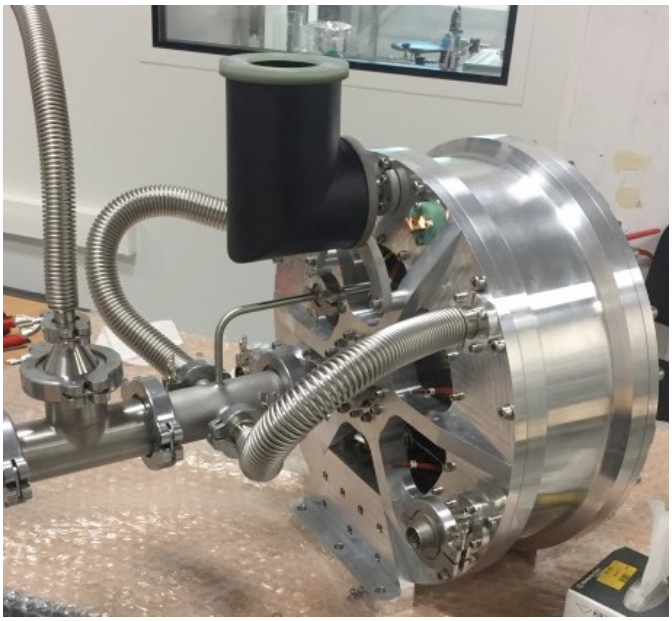

Figure 3. The 50 kW HTS motor

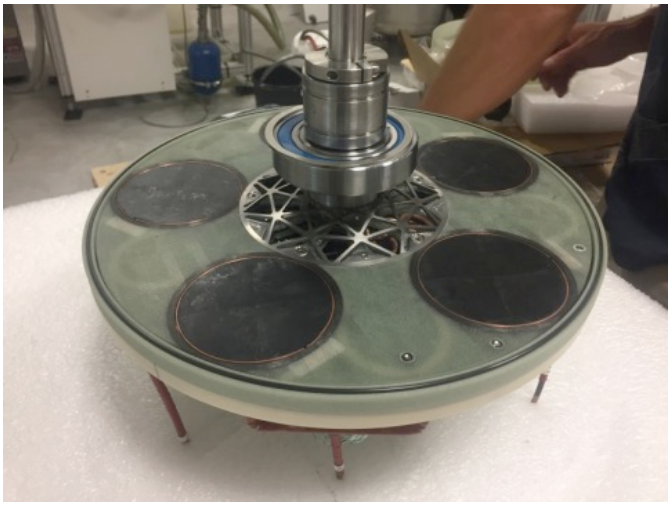

Figure 4. The rotor of the 50 kW HTS motor

3. Test setup & instrumentation

The prototype of the 50 kW machine is connected to an in-duction motor. The connection between the two machines is made with a flexible coupling in order to eliminate some of the vibrations of the asynchronous motor. The motor is driven by a 3-phases inverter connected to the grid. Figure 5 shows a picture of the test stand; the cryogenic cooling system does not appear on this figure.
For the first tests, only one armature winding has been in-stalled. This operation allows to approach a Hall effect probe near the pellets (to the thickness of the vacuum and the cryo-stat) and thus measure the modulation of the magnetic flux.

Figure 6 shows the location of the different temperature probes on the HTS coil. There is a total of 3 PT100s, 2 for the helium exchanger (inlet and outlet) and 1 on the copper thermal bus. As the superconducting pellets are part of the rotor, it was not possible to monitor their temperatures.

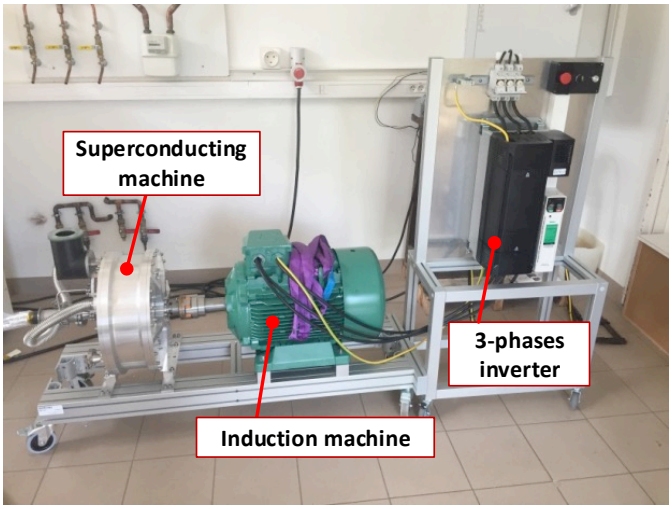

Figure 5. Test stand of the HTS prototype

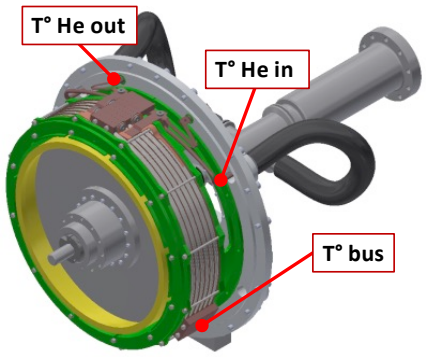

Figure 6. Measure of the temperature of the HTS coil

4. First test of the prototype

4.1. Cool down

Figure 7 shows the cooling of the superconducting coil (T° bus) which is about 4 hours to reach a temperature of 33 K. The temperature of the helium at the inlet and outlet of the ex-changer with the coil is also shown in this figure. The rapid drop in temperature at the beginning of cooling is due to the process of starting. Indeed, the cold head's compressor (CP1100) was powered first. When the second compressor (CP380) was started, the temperature of the cold head was al-ready below 200 K.

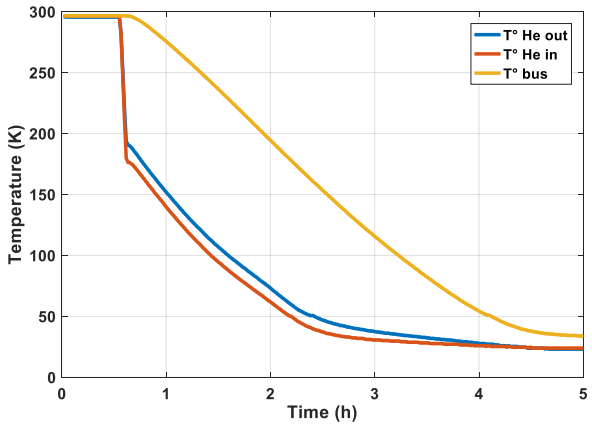

Figure 7. Plot of different temperature sensor with time

4.2. Flux modulation

The modulation of the magnetic field is shown in figure 8a, b and c at the mean radius for 3 different currents in the SC coil (50 A, 100 A and 120 A).

First of all, we can see that the numerical model is quite ac-curate in terms of the variation of the magnetic field between the HTS pellets (maximum value). In our numerical model, we considered that the HTS pellet has homogeneous proper-ties with a current density Jc=2250 A/mm² according to [13]. However, behind a SC pellet, there is an area where the magnetic field "penetrates" into the superconductor. This is explained by the manufacture of the HTS pellet which consists of 4 germs. It appears at the growth boundary an area where the performance of the superconductor is lower. This is shown in figure 9a. This behaviour can be modelled by a second numerical approach by considering a current density Jc2 lower than the current density Jc1 of the single crystal. A simulation result is shown in figure 8c and figure 9b on the penetration of the magnetic field to explain this phenomenon. It can be

seen that by taking Jc1 = 2250 A/mm² and Jc2 = 30 A/mm², the numerical results are comparable with the experimental results.

4.3. No-load tests

Figure 10 shows the phase-to-phase voltages measured for one armature winding when the superconducting coil is sup-plied with a current I of 120 A (half of the critical value) and the machine is rotating at a speed N of 250 rpm (1/20 of the nominal speed due an unbalanced bench during this test). We can notice the sinusoidal shape of these voltages.

As the thin back-iron is rapidly saturated, we can make linear extrapolations. When multiplied by 20 (nominal speed 5000 rpm), then by 2 (critical current of the HTC coil) and finally by 2 (the two armatures winding on each side in series), we obtain a maximum voltage between 296 V and 316 V, instead of the 535 V (phase-to-phase) initially planned. There are several explanations for this significant voltage difference:

- The modulation of the flux is not in accordance with the theory due to the penetration of the magnetic field at the HTS pellet's growth boundaries, see Fig. 9, which reduces the flux through the armature coils.
- Due to the construction feasibility, the air-gap length and the number of turns for the armature winding was slightly modified from the theoretical design.

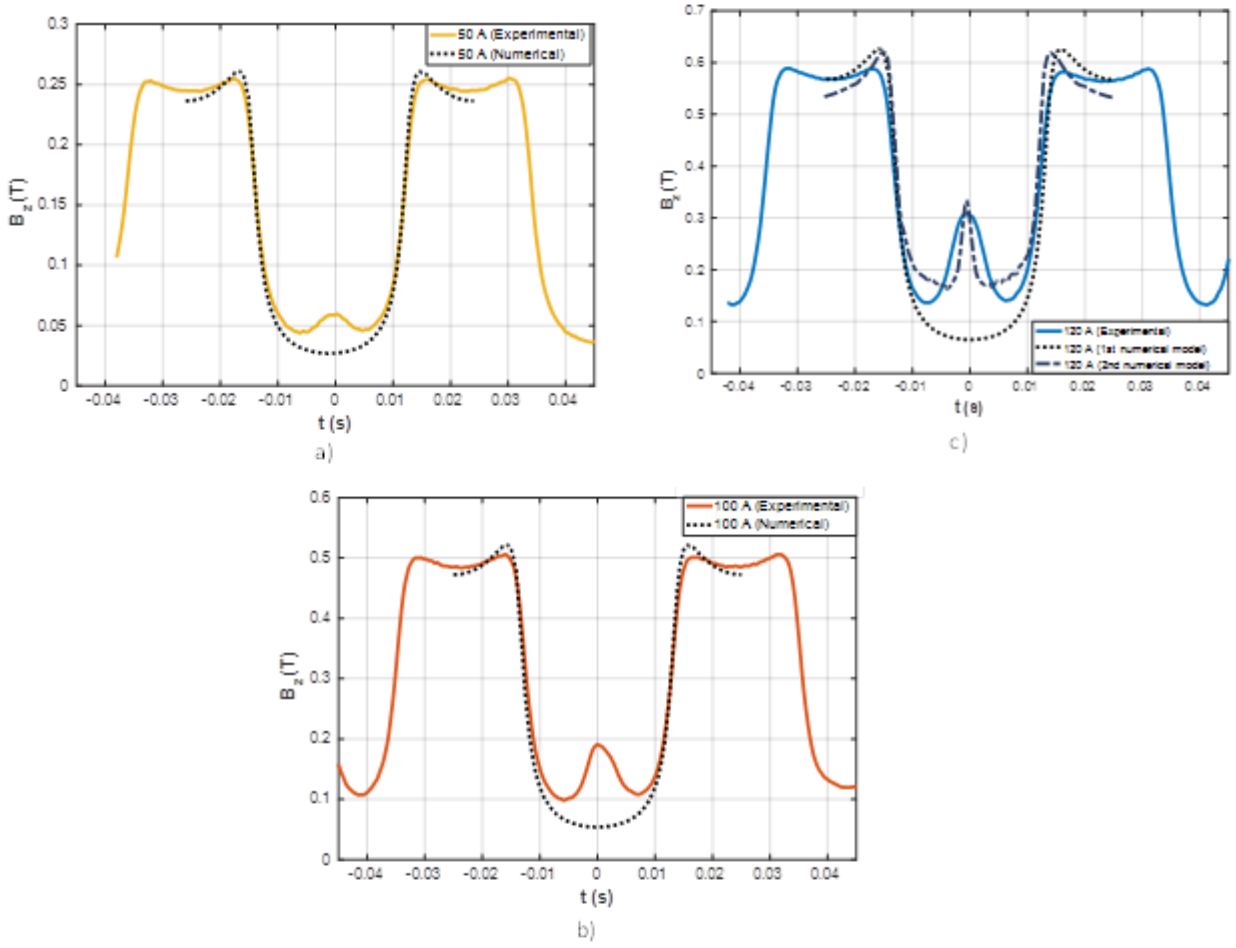

Figure 8. Flux modulation for 3 different current in the HTS coil: a) 50 A b) 100 A and c) 120 A (also with the results of figure 9)

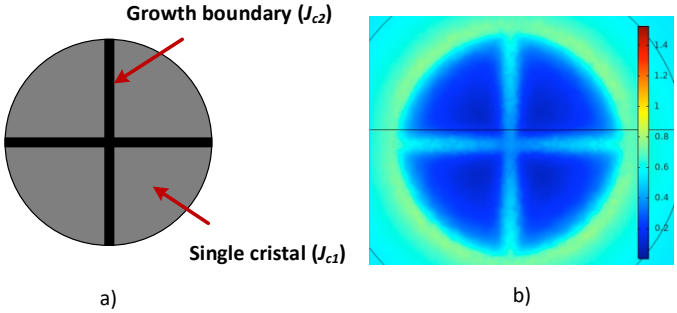

Figure 9. a) Scheme of a multi-germ HTS pellet b) Magnetic modulation with $J_{c1} = 2250\ A/mm^2$ and $J_{c2} = 30\ A/mm$

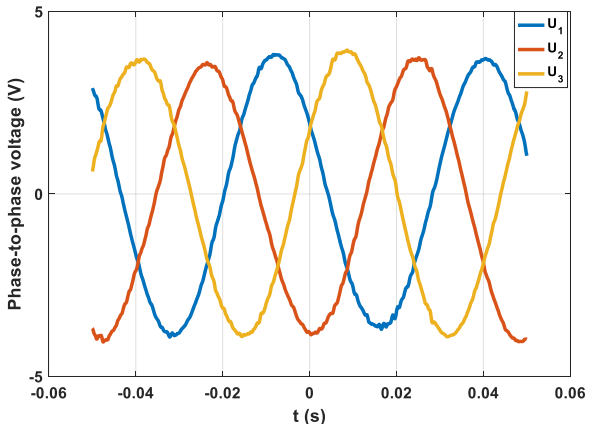

Figure 10. Phase-to-phase voltage of one armature winding for I = 120 A and N = 250 rpm

5. Conclusion

A 50 kW designed prototype with the objective of reducing the mass was manufactured. This is why lightweight materials such as aluminium have been used for cryostats. The final weight of the machine is estimated at around 52 kg. However, a significant reduction in weight can still be achieved on non-active parts such as cryostats, flanges, etc.

Finally, the first tests of the machine allowed to partially validate the modulation of the magnetic field with the HTS multiseed pellets. We observed a penetration of the magnetic field at the growth boundary. This effect deteriorates the induced voltage in the armature winding. This phenomenon had been underestimated because of the low temperature of the pellets obtained by cooling.

For the moment, no load tests have been carried out. The superconducting coil could not be supplied with an excitation current greater than 120 A. Because beyond that, the magnetic interaction of the machine's axial field on the ferrofluid seal breaks the vacuum, resulting in very rapid heating of the machine.

Acknowledgments

The author would like to thank the Direction Générale de l'Armement (DGA), "Projet ANR- RF-2013-01", for it support and interest.

References

[1] J. L. Felder, Marsh 2017, 'NASA electric propulsion system studies. Report No. GRC-EDAA-TN28410, 2015, Available at ntrs.nasa.gov.

[2] 2016, National Academies of Sciences, Commercial Aircraft Propulsion and Energy Systems Research: Reducing Global Carbon Emissions.
[3] K. S. Haran et al., 2017, « High power density superconducting rotating machines—development status and technology roadmap », *Supercond. Sci. Technol.,* **vol. 30***, no 12, p. 123002, 2017*.
[4] C. A. Luongo et al., 2009, « Next Generation More-Electric Aircraft: A Potential Application for HTS Superconductors », *IEEE Transac-tions on Applied Superconductivity*, vol. **19**, no 3, p. 1055 1068.
[5] P. J. Masson, G. V. Brown, D. S. Soban, et C. A. Luongo, 2007, « HTS machines as enabling technology for all-electric airborne vehicles », *Supercond. Sci. Technol.*, vol. **20**, no 8, p. 748.
[6] J. L. Felder, 2011, « Turboelectric Distributed Propulsion in a Hybrid Wing Body Aircraft », in *20th International Society for Airbreathing Engines*, Gothenburg, Sweden.
[7] G. Brown, 2011, « Weights and Efficiencies of Electric Components of a Turboelectric Aircraft Propulsion System », in *49th AIAA Aerospace Sciences Meeting*, American Institute of Aeronautics and Astronautics.
[8] M. Feddersen, K. S. Haran, et F. Berg, 2017, « AC Loss Analysis of MgB2-Based Fully Superconducting Machines », *IOP Conf. Ser.: Mater. Sci. Eng*., vol. **279**, no 1, p. 012026.
[9] K. Berger et al., july 2017 « Benchmark on the 3D Numerical Modelling of a Superconducting Bulk », *IEEE Compumag*.
[10] A. Colle, T. Lubin, S. Ayat, O. Gosselin, et J. Lévêque, dec 2019, « Analytical Model for the Magnetic Field Distribution in a Flux Modulation Superconducting Machine », *IEEE Transactions on Magnetics*, vol. **55**, no 12, p. 1 9.
[11] F. Marignetti, G. Tomassi, P. Cancelliere, V. D. Colli, R. D. Stefa-no, et M. Scarano, 2006, « Electromagnetic and Mechanical design of a Fractional-slot-windings Axial-flux PM synchronous machine with Soft Magnetic Compound Stator », in *Conference Record of the 2006 IEEE Industry Applications Conference Forty-First IAS Annual Meeting*, vol. 1, p. 62 69.
[12] T. Trollier, J. Tanchon, Y. Icart, et A. Ravex, 2014, « High capacity 30 K remote helium cooling loop », *AIP Conference Proceedings*, vol. 1573, no 1, p. 1461 1466.
[13] Z. Deng et al., 2014, « Trapped flux dependence of bulk high-temperature superconductors between 77 and 30 K under a limited excitation field », *Journal of Superconductivity and Novel Magnetism*, vol. **27**, no 6, p. 1413–1417.